Encoding of Motion Targets by Waves in Turtle Visual Cortex

Xiuxia Du*, Bijoy K. Ghosh, *Fellow, IEEE*, and Philip Ulinski

***Abstract*—Visual stimuli evoke wave activity in the visual cortex of freshwater turtles. Earlier work from our laboratory showed that information about the positions of stationary visual stimuli is encoded in the spatiotemporal dynamics of the waves and that the waves can be decoded using Bayesian detection theory. This paper extends these results in three ways. First, it shows that flashes of light separated in space and time and stimuli moving with three speeds can be discriminated statistically using the waves generated in a large-scale model of the cortex. Second, it compares the coding capabilities of spike rate and spike time codes. Spike rate codes were obtained by low-pass filtering the activities of individual neurons in the model with filters of different band widths. For the moving targets used in the study, detectability using spike rate codes is immune to the choice of a specific bandwidth, indicating that a coarse filter is able to adequately discriminate targets. Spike timing codes are binary sequences indicating the precise timing of spike activity of individual neurons across the cortex. Spike time codes generally perform better than do spike rate codes. Third, the encoding process is examined in terms of the underlying cellular mechanisms that result in the initiation, propagation and cessation of the wave. The period of peak detectability corresponds to the period in which waves are propagating across the cortex.**

***Index Terms*—β-space representation, Karhunen-Loeve (KL) decomposition, motion encoding, Statistical hypothesis testing, turtle visual cortex.**

I. Introduction

VISUAL inputs produce waves that propagate across the visual cortex of freshwater turtles and visual information is encoded in the cortical waves ([1]–[3]). Nenadic, *et al.* [4] used a large-scale model of the cortex and a two-step Karhunen-Loeve (KL) decomposition to show that the locations and speeds of visual targets can be discriminated from the dynamics of these waves. The first decomposition represents the cortical wave as a linear combination of spatial modes with time-varying coefficients. The cortical wave is, thus, represented by a trajectory in a phase space called the A-space. Most of the energy contained in the original wave can be captured by the decomposition coefficients corresponding to the first three principal modes. A further reduction of the dimensionality of the wave is achieved by a second KL decomposition which maps the A-space trajectories onto points in a low-dimensional space called the B-space. The two-step KL-based representation introduced by Nenadic *et al.* [4] has been further refined by Du *et al.* [5] to emphasize how visual targets are encoded in the B-space in the form of a strand (called a β-strand), wherein each point of the strand represents a specific time window. The analysis shows how strands can be used to detect and discriminate between alternative visual targets.

This paper extends the discrimination analysis using β-strands to include moving and double-input-with-time-delay visual targets. Each gives rise to a spatiotemporal pattern of visual signals and the paper establishes how these signals can be detected statistically using a Bayesian approach and by calculating the maximum likelihood. The results obtained are qualitatively similar to those obtained earlier [5] for stationary targets. Second, the paper shows that the motion cues are reliably coded by low frequency components (e.g., a rate code) of the evoked cortical waves, but that the time-coded signals are able to detect moving targets over a larger window and yield a better detection performance. A final contribution of the paper is to establish how target detectability, as measured by the probability of classification error, is affected by initiation and propagation of the cortical wave. Our simulations using the model cortex show that target encoding in the model cortex is carried out in three phases. Parameters from the moving target are integrated during the initiation phase I, retained by the propagating waves in the cortex during propagation phase II and fade away as cortex becomes hyperpolarized during the wave cessation phase III. The optimal detection window falls during phase II when the already encoded motion cues are retained by the cortical waves.

II. Input Detection With the Bayesian Method

A. A Brief Description of the Cortex Model

The model of the visual cortex considered in this paper was described in detail by Nenadic *et al.* [6]. Briefly, it consists of 744 cortical neurons and 201 dorsal lateral geniculate neurons (LGNs). Pyramidal cells constitute the largest population of neurons in the model (368 lateral and 311 medial pyramidal neurons). The remaining cells are two types of inhibitory interneurons (45 stellate and 20 horizontal neurons). Cortical neurons are distributed in a two-dimensional (2-D) array that captures the spatial distribution of the three major populations of cortical neurons. Fig. 1 shows the spatial structure of the model. Each neuron is represented by a multicompartmental model based on the anatomy and physiology of that type of cortical neuron. The soma compartment of each model neuron

Manuscript received September 30, 2004; revised February 25, 2006. This work was supported in part by the National Science Foundation (NSF) through the Collaborative Research Computational Neuroscience Program under Grant EIA-0218186 and through the Control, Networks, and Computational Intelligence Program under Grant ECS-0323693. *Asterisk indicates corresponding author.*

X. Du is with the Pacific Northwest National Laboratory, Fundamental Science Division, 2500 George Washington Way, Richland, VA 99352 USA (e-mail: xiuxia.du@pnl.gov).

B. K. Ghosh is with Washington University, St. Louis, MO 63130 USA.

P. Ulinski is with the University of Chicago, Chicago, IL 60637 USA.

Digital Object Identifier 10.1109/TBME.2006.877796

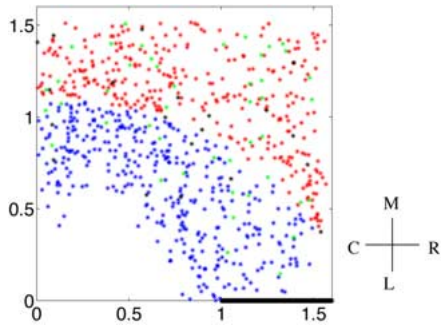

Fig. 1. Spatial structure of the cortex model. 744 cortical cells are distributed as a 2-D array. Lateral pyramidal cells, medial pyramidal cells, stellate cells, and horizontal cells are shown in blue, red, green and black, respectively. A cortical neuron is synaptically connected to all post-synaptic cortical neurons positioned within a sphere of influence. A total of 201 LGNs, shown in black, are aligned linearly along the lateral edge of the cortex. The dimensions are in millimeters.

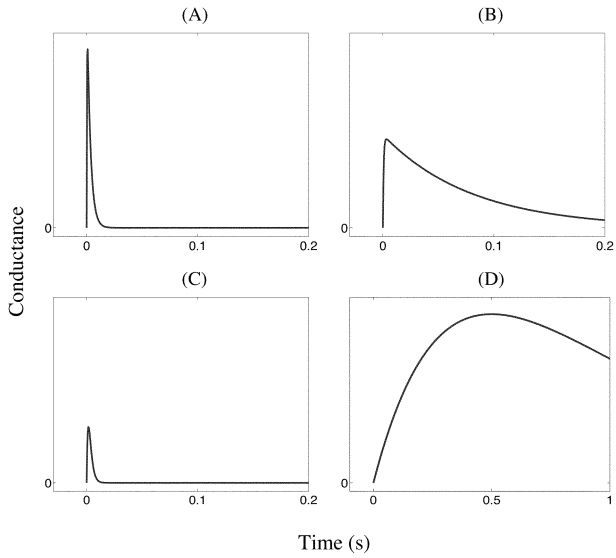

Fig. 2. Time course of activated synaptic conductances. AMPA ergic and NMDA ergic synaptic conductances follow a dual exponential function and GABA_A ergic and GABA_B ergic conductances follow an alpha function. Note that each conductance is scaled differently in the model. The time scale of GABA_B ergic conductance is different in the figure from the time course of other conductances. (A) AMPA ergic conductance. (B) NMDA ergic conductance. (C) GABA_A ergic conductance. (D) GABA_B ergic conductance.

contains voltage-gated conductances sufficient to generate action potentials. Excitatory (AMPA and NMDA) and inhibitory (GABA_A and GABA_B) synaptic conductances establish interactions between individual neurons. Synaptic connections between neurons are established according to a predefined sphere of influence. Geniculate neurons are arranged in a row along the lateral edge of the cortex. Each geniculate neuron is modelled as a single compartment with ionic currents that generate action potentials following the injection of a stimulating current in the neuron. Synaptic contacts between geniculate and cortical neurons occur at the site of varicosities.

LGNs contact cortical neurons via AMPA ergic synapses. Pyramidal cells contact cortical neurons by simultaneous activation of both AMPA ergic and NMDA ergic receptors. Inhibitory neurons contact cortical neurons by simultaneous activation of GABA_A ergic and GABA_B ergic receptors. The time courses of the AMPA ergic and NMDA ergic conductances are specified using dual exponential functions

$$g_{\mathrm{syn}}(t) = g_{\max}/(\tau_1 - \tau_2)(e^{-t/\tau_1} - e^{-t/\tau_2}) \tag{1}$$

with $\tau_1 = 3$ ms and $\tau_2 = 0.3$ ms for AMPA ergic synapses and $\tau_1 = 80$ ms and $\tau_2 = 0.67$ ms for NMDA ergic synapses. The time course of GABA_A ergic and GABA_B ergic synaptic conductances are specified using alpha functions

$$g_{\mathrm{syn}}(t) = g_{\max}\frac{t}{\tau}e^{1-t/\tau} \tag{2}$$

with $\tau = 1.7$ ms for GABA_A ergic and $\tau = 500$ ms for GABA_B ergic synapses. Fig. 2 shows the time courses of the four synaptic conductances. Each conductance is scaled by a synaptic weight which is specified by either a uniform base synaptic weight within the sphere of influence or a weight that decreases exponentially following a Gaussian function (see [6]).

B. Simulation Experiments

Moving and double-input-with-time-delay stimuli were simulated by injecting current pulses into LGNs. Moving stimuli were simulated by activating the left-most 100 adjacent LGN neurons, from left to center, with a sequence of square current pulses of equal amplitude and duration that were delayed with respect to each other. The amplitude and duration of each current pulse were 0.3 nA and 30 ms, respectively. For each moving stimulus, the delay between adjacent current pulses was equal and the magnitude of the delay determined the speed of the stimulus. Three stimulus velocities were used and were denoted as S (slow), M (medium), and F (fast). The three moving stimuli were parameterized by the delay of one square pulse with respect to its neighbor. The delays for the slow, medium, and fast moving stimuli were 1.3 ms, 0.91 ms, and 0.47 ms, respectively.

Double-input-with-time-delay stimuli were simulated by presenting two square current pulses to two groups of adjacent LGNs. The amplitude and duration of the pulses were the same as those of the pulses simulating a moving stimulus. One group, denoted as L (left), consisted of the leftmost 20 adjacent LGN neurons and each LGN in the group was stimulated by the first square current pulse. The other group, denoted as R (right), consisted of the rightmost 20 adjacent LGN neurons of the array and each LGN received the second current pulse. Both the current pulses had the same amplitude and duration, but the second pulse was delayed with respect to the first. Three time delays were considered: 40, 80, and 120 ms. The two locations of the LGN groups and the three time delays between the two current pulses gave twelve different combinations of the inputs: LL40, LL80, LL120, LR40, LR80, LR120, RL40, RL80, RL120, RR40, RR80, and RR120. The symbol LR40 means that the left group of LGN neurons received the first current pulse and the right group of LGN neurons received the second pulse, which was delayed 40 ms after the first pulse.

The stochastic nature of the action potential generation and the noisy environment that neurons live in were simulated by injecting noisy current into the soma of each cortical neuron at

each simulation step of 0.05 ms. Noise current was governed by a Gaussian distribution with a mean of 0 and a standard deviation of 4 nA. A saturation threshold was set to restrict the noisy current within the range of ± 12 nA. For each stimulus, the cortex model produced 50 sample propagating waves. A total of 150 and 600 waves were generated for moving and double-input-with-time-delay stimuli, respectively. The length of the simulation time was 1 000 ms and the sampling frequency was 1 KHz.

C. Input Detection Method

Cortical waves have been analyzed as a Bayesian problem by Du *et al.* [5]. Briefly, each movie was split up into a sequence of overlapping 10 ms encoding windows. Within each window, the movie was projected as a point using double KL decomposition in a suitable low-dimensional B-space. The sequence of points in the B-space gave rise to a strand, called a β-strand. Each cortical wave was represented as a vector-valued time series given by the β-strand and the detection task was to discriminate strands originating from different inputs. In this way, the problem was reduced to a Bayesian problem. Expanding detection windows (EDWs) and sliding detection windows (SDW) were applied over the β-strand. The combination of encoding and decoding windows made it possible to localize visual targets in space.

In [5], we considered three alternative hypotheses and the problem was to discriminate between three stationary flashes located at equally spaced locations along the horizontal axis of the visual field. The goal of this paper is to discriminate between three different target velocities moving from left to the center of the visual field, and between double flashes separated in time and occurring at the same or different regions of the cortex. For the three-hypotheses testing problem, we computed two logarithm likelihood ratios corresponding to the posterior probability density of the visual cue conditioned on the β-strand. A 2-D decision space was constructed and divided into three regions based on the two likelihood ratios. Each arbitrary β-strand was represented as a point in the decision space; the region into which the point fell determined the input. When the number of hypotheses is more than three (12 in the case of double-input-with-time-delay stimuli considered in this paper), the dimension of the decision space is higher than 2 and it is not possible to visualize the space. However, we can continue to use the Bayes criteria and assume that the cost of a correct decision is zero and the cost of every wrong decision is the same. We can then compute the likelihood function

$$l_i(\mathbf{R}) = \ln P_i - \frac{1}{2}\ln|\mathbf{K}_i| - \frac{1}{2}(\mathbf{R}-\mathbf{m}_i)^T\mathbf{Q}_i(\mathbf{R}-\mathbf{m}_i)$$

where, $\mathbf{R}$ is the projection vector of a given, observed sample β vector, P_i is the *a priori* probability of the ith hypothesis, $\mathbf{m}_i$ is the mean of $\mathbf{R}$ corresponding to the ith hypothesis, $\mathbf{K}_i$ is the covariance matrix of the noise corresponding to the ith hypothesis, and $\mathbf{Q}_i = \mathbf{K}_i^{-1}, i = 1,2,\ldots,M$. The algorithm predicts the ith hypothesis to be most likely if $l_i(\mathbf{R})$ takes on the maximum value (See [5] and [7] for details).

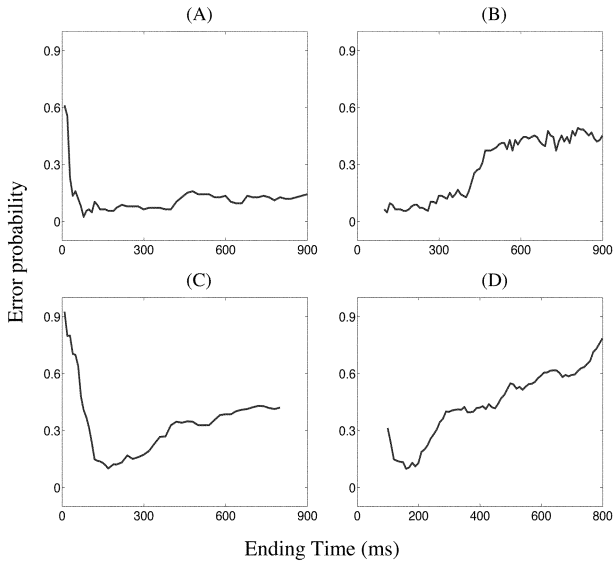

Fig. 3. Detection error probability as a function of the ending time of time windows. (A) Error probability for detecting the speeds of the moving stimuli by EDW approach. (B) Error probability for detecting the speeds of the moving stimuli by SDW approach. (C) Error probability for detecting the double-input-with-time-delay stimuli by EDW approach. (D) Error probability for detecting the double-input-with-time-delay stimuli by SDW approach.

D. Detection Performance Analysis

Detectability for moving and double-input-with-time-delay stimuli is shown as detection error probability curves in Fig. 3. The curves plot the probability of making a detection error as a function of time. A detection error occurs when a point in the decision space crosses the separation boundary between two hypotheses of the decision space and falls in a region corresponding to an incorrect hypothesis. Fig. 3(A) and (B) shows the detection error probability in detecting three speeds for moving stimuli using EDWs and SDWs, respectively. In Fig. 3(A), the window of detection is expanding and, in general, information in the wave is retained as a function of time. A close-to-zero detection error probability is achieved at around 70 ms and rises to about 15% at 900 ms. In Fig. 3(B), a window of width 100 ms is sliding in time. The detection error remains close to zero until about 400 ms and rises to about 50% for a window with a terminal time at about 900 ms. This indicates that there is practically no information about the input contained in this part of the wave because a random guess would give a detection error probability of about 66% if each speed occurs with a probability of 0.33. Likewise, Fig. 3(C) and (D) shows the detection error probability for detecting 12 double-input-with-time-delay stimuli. As in figures Fig. 3(A) and (B), the detection error declines until about 150 ms and increases thereafter. The concave shape of the detection error probability curves indicates that there is an optimal time period when discrimination is the best. The detection error probability is large at 0 ms in each case. It then declines approximately linearly to a minimum (around 150 ms in Fig. 3(C) and (D)) and slowly increases for longer times.

In Fig. 4(A)–(D), the detection error probability has been plotted as a function of time for detecting the time delay (40 ms, 80 ms, and 120 ms) between two double-input-with-time-delay

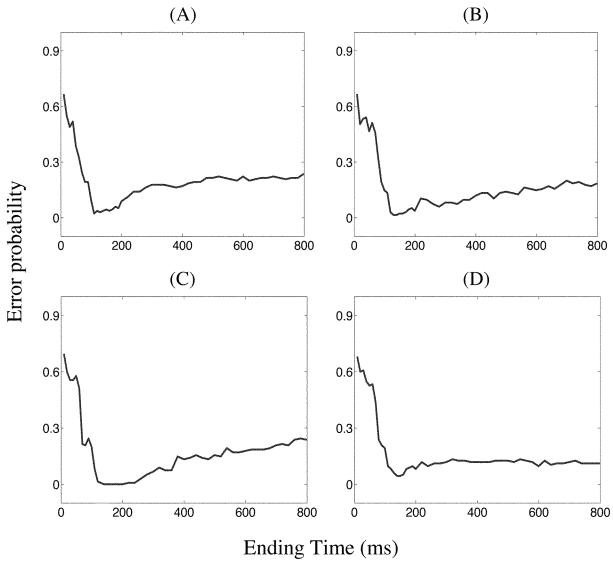

Fig. 4 Errorprobability for detecting the time delay between the two current pulses in the double-input-with-time-delay stimuli. The detection is performed using EDW approach. (A) Detection errorfor detecting time delay when the inputs are located both in the left. (B) Detection error for detecting time delay when the first input is from the left and the second is from the right. (C) Detection error for detecting time delay when the first input is from the right and the second is from the left. (D) Detection error for detecting time delay when both inputs are from the right.

visual stimuli. The different plots in Fig. 4 refer to different locations of the visual input. As in Fig. 3(A) and (C), the curves refer to an EDW and the shape continues to remain concave. The probability of error attains a minimum and remains bounded below 30% at later times.

III. Spike Rate Versus Spike Timing Encoding

The fact that we were able to discriminate inputs using EDWs and SDWs demonstrates that spike rate is an effective information carrier in the cortex model used in this paper. However, the exact times when a single neuron fires or when a population of neurons fires action potentials can encode information in different cortical areas in a variety of species. This section, thus, compares the effectiveness of a spike timing code to a spike rate code at different resolutions.

A. Input Detection With Spike Rate Coding

The spike rate signal was obtained from the spike trains with a low-pass filter described by

$$y = kte^{-t/\tau} \tag{3}$$

where $k = 0.18$ is a constant. τ is the time when y reaches its maximum and determines the width of the filter. A larger τ corresponds to a larger window in which to count spikes and, thus, the spike rate signal will be coarser. Fig. 5 shows the low-pass filters with 11 equally spaced τ's. The values of τ are between 0.005 and 0.05 with a step 0.0045. The spike rate signals of a spike train corresponding to 6 of the 11 τ values are shown in Fig. 6. The β-strand representation of the filtered waves were

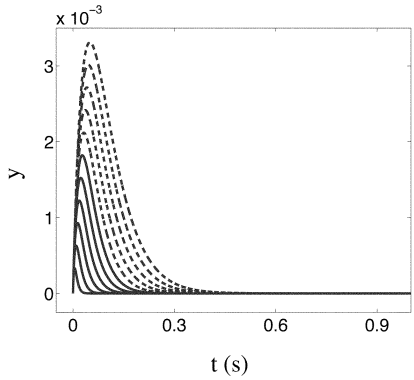

Fig. 5. Time-domain representations of low-pass filters of different widths as described in Eqn. (3).

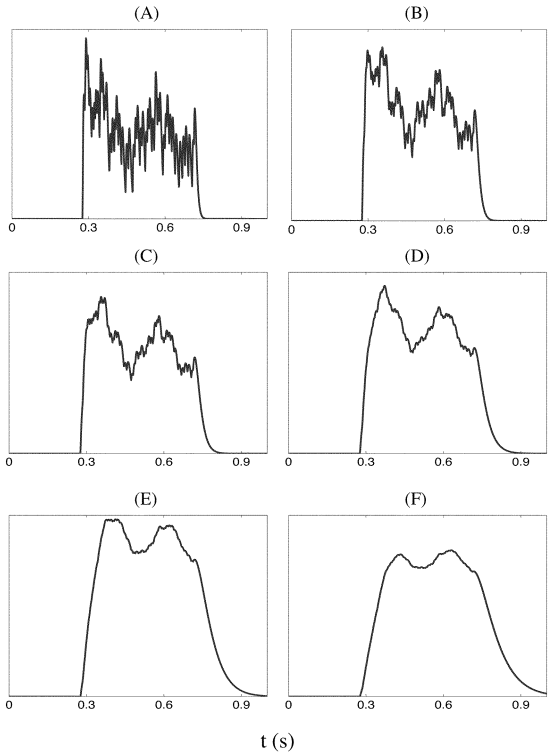

Fig. 6. Spike rate signals of a spike train at different resolution. Each spike rate signal was obtained by passing the original spike train through a low-pass filter. The smaller the filter width, the higher resolution the spike rate signal has. From (A) to (E), the filter width gradually increases.

calculated and the hypothesis testing algorithm was used to discriminate the inputs for each of the 11 different τ's. To see the effect of τ on the detection performance, the total number of detection errors was obtained by summing the detection errors across the detection windows for each τ. Fig. 7(A) and (B) shows the total number of detection errors versus τ for EDWs and SDWs, respectively. The effect of τ on the detection performance is negligible. This result is surprising at first glance, since the spike rate signals corresponding to different τ's are the spike rate signals of the spike train at different resolutions. Intuitively, the finer the resolution, the more information the corresponding spike rate signal should contain and, thus, the better detection performance. However, this result is actually expected from the

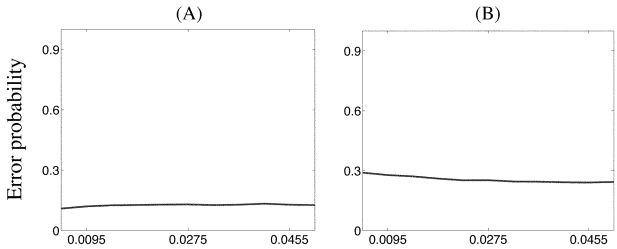

Fig. 7. Error probability of input detection versus filter width τ for (A) EDW approach and (B) SDW approach.

data processing procedure used in calculating the β-strand representation for the Bayesian detection. The spike rate signal obtained from a narrower filter undoubtedly retains more information from the original spike train. However, we have discarded some information about the input by using only those β coefficients that correspond to the first few principal components in the double KL decomposition process and only those dominant projection coefficients in the β-strand whitening process (See [5]). So, even if the spike rate signals corresponding to the different filters contain different amounts of information about the input, the coefficients that were ultimately used to perform Bayesian detection contained approximately similar amounts of information. This resulted in the similar detection performances for different τ's.

B. Input Detection With Spike Timing Coding

Since the Bayesian hypothesis testing algorithm used only part of the information contained in the original spike train and, on the other hand, the spike timing information of individual neurons is not completely reliable, we wanted to examine the detection performance based on the spike timing of all the cortical neurons. The spike timing of a neuron was obtained by dividing its spike train into non-overlapping, equal-length bins and assigning either a 0 or 1 to each bin. Each bin was 1 ms long. A value of 1 was assigned to the bin if a spike occurred in the bin and 0 otherwise. A spike train was, thus, converted to a binary sequence of 0's and 1's and the spike timing pattern of all the cortical neurons was represented by a binary matrix. Each row of the matrix corresponded to a particular neuron and each column of the matrix corresponded to a particular bin. Double KL decomposition was performed to obtain the β-space representation of the spike timing matrix. The average β-strand was obtained for each type of the moving and double-input-with-time-delay input stimuli. Input discrimination based on spike timing was different from that based on the spike rate. Rather than using the Bayesian approach, a Euclidean distance was calculated between the β-strand representation of a given wave and the average β-strand representation of each possible input. The smallest of these distances indicates which input most likely had produced the given cortical wave. Fig. 8(A) and (B) shows the detection performance in detecting the moving and double-input-with-time-delay stimuli, respectively. A comparison with Fig. 3 indicates that the input detection based on spike timing patterns yields a better detection performance. This indicates that the spike timing patterns of the cortex model considered in this paper are reliable enough to enable reasonable

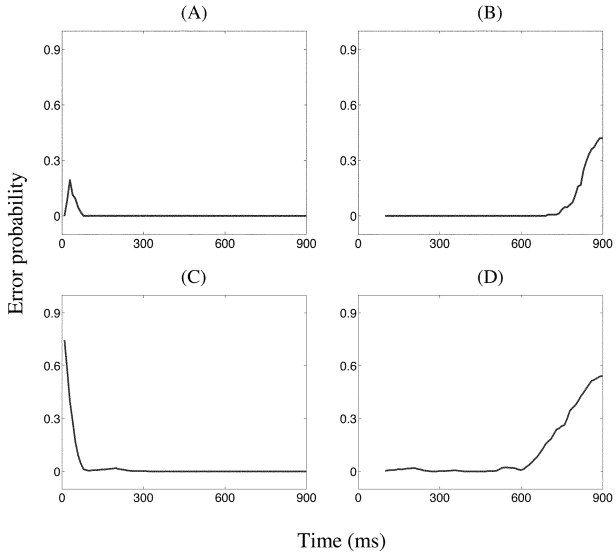

Fig. 8. Detection error probability based on spike timing patterns of the cortex. (A) Detecting moving stimuli using EDW. (B) Detecting moving stimuli using SDW. (C) Detecting double-input-with-time-delaystimuli using EDW. (D) Detecting double-input-with-time-delay stimuli using SDW.

detections, and the spike timing patterns carry more information about the input than does the spike rate.

IV. The Three Phases of Input Detection

The detection performances shown in Figs. 3 and 4 indicate that the information content of the wave evolves with time. It is low at the beginning of wave formation, increases and reaches a peak, and then gradually decreases. Regardless of the input that has induced it, the cortical wave consists of three phases: initiation, propagation, and cessation. This section relates the evolution of the detection performance to the three phases of the wave. The three phases are illustrated in the case of a moving stimulus in Fig. 9.

A. Phase I: Wave Initiation

A visual stimulus reaches the cortex via LGNs which make AMPA ergic synapses on cortical neurons. The geniculocortical synaptic connections occur at the varicosities along geniculate axons (see [6]). During the phase of wave initiation, the spatiotemporal characteristics of the input are encoded into the initial spatiotemporal pattern of depolarization in the cortex. For example, the moving stimulus considered in this paper activated the left-most 100 LGNs and each LGN produced two spikes. The cortical neurons that were postsynaptic to these LGNs were depolarized. The locations of these lateral pyramidal, medial pyramidal, and stellate cells are shown in Fig. 10. The faster the moving stimulus, the faster the LGNs fired action potentials, and the faster the initial depolarization was produced in the cortex. The spatial characteristics of the input were reflected in the locations of those activated LGNs and, consequently, in the spatial distribution of the initial depolarization. Due to the time delay from input onset to activation of the LGNs and then to the depolarization of the cortex, the input stimulus was encoded in the cortex over time and the information content of the input in the wave increased gradually. Consequently, the input detection

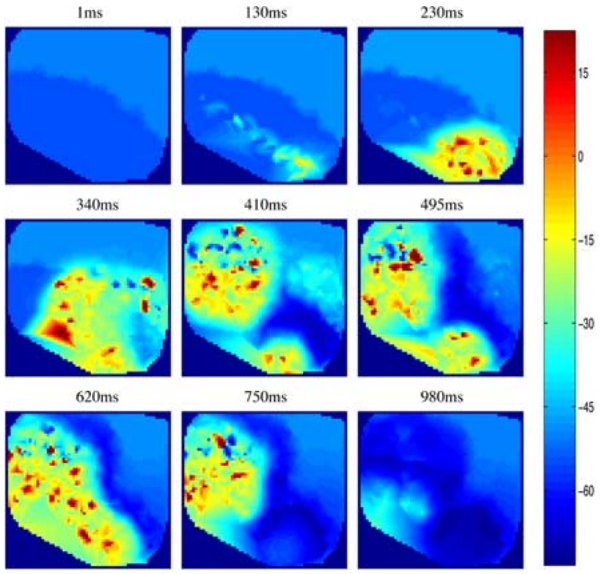

Fig. 9. Wave initiation, propagation, and cessation. A moving input stimulus initiates the wave at the lateral-rostral corner of the cortex. The wave propagates initially in all directions due to the sphere of influence. After the inhibitory synaptic conductances are activated, the wave propagates across the cortical regions where excitation dominates inhibition. Wave cessation is a result of the cortex hyperpolarization and its propagation.

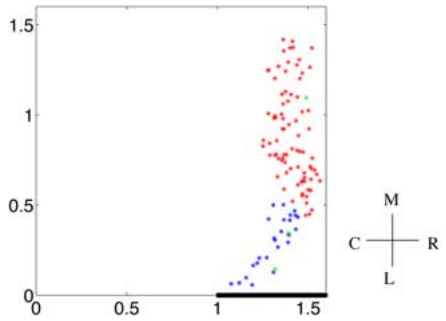

Fig. 10. Spatial distribution of cortical cells activated by a moving stimulus. A moving stimulus was simulated by injecting a square current pulse sweeping across the left-most 100 LGNs. Lateral pyramidal, medial pyramidal, and stellate cells are shown in blue, red, and green, respectively.

performance improved with time and the detection error probability decreased monotonically, as seen in Figs. 3 and 4. Further propagation of the initial depolarization is dictated by the cortical organization. Specifically, both the sphere of influence and the spatiotemporal profiles of the synaptic conductances play a crucial role in spreading the depolarization over the cortex.

B. Phase II: Wave Propagation

Wave propagation follows a particular path dictated by the relative spatial density of the excitatory and inhibitory synaptic conductances in the cortex. Fig. 11 shows the spatial density of the ratio of the excitatory (the sum of AMPA ergic and NMDA ergic conductances) to GABA_A ergic conductance. It shows that there is a belt that extends from the lateral-rostral to the medial-caudal edge of the cortex and in which excitation dominates inhibition. Since the initial depolarization induced by the input stimulus usually occurs in the lateral-rostral corner, the wave propagates toward the medial-caudal edge of the cortex

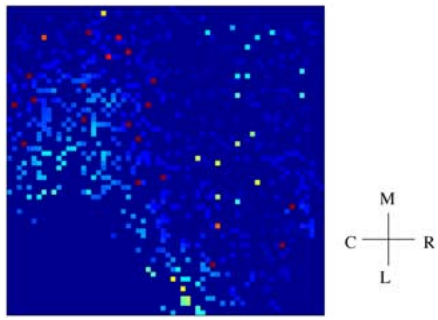

Fig. 11. Spatial density of the ratio of excitatory to GABA_A ergic conductance in the cortex. The magnitude of the ratio is color-coded, with the bright color representing larger values of the ratio. The bright areas are dominated by excitatory synaptic conductances and the dark areas are dominated by inhibitory synaptic conductances.

along the excitation-dominant belt. The temporal properties of the synaptic conductances cause the wave to propagate in one direction. The GABA_B ergic synaptic conductance has a longer time constant than that of the excitatory synaptic conductances (Fig. 2). Thus, a cortical region that has just been depolarized is subsequently hyperpolarized, which prevents the wave from propagating back to its source of origin. Information about the input that was encoded into the wave during the phase of wave initiation is retained in the wave. During wave propagation, neurons are dynamically depolarized and hyperpolarized due to the input and, consequently, input information is reflected in the spatiotemporal pattern of the cortex depolarization and hyperpolarization. Signal-to-noise ratio (SNR) is the highest during this time period and detection is able to achieve an optimal performance.

C. Phase III: Wave Cessation

The visual inputs used in the paper are shorter than the durations of the waves they produce. A moving stimulus lasted 30 ms and the longest double-input-with-time-delay input was 180 ms. The waves persisted after the stimulus was finished. However, inhibition mediated by GABA_A ergic and GABA_B ergic synapses gradually hyperpolarized the cortex, which resulted in a gradual fading of the wave. The information content of the wave gradually decreases during wave cessation because each neuron was subjected to the same amount of noisy current as at the beginning of the wave, the SNR of the system decreases and the cortex is gradually taken over by noise. The input detection performance deteriorates and the detection error probability, accordingly, increases. Since the lateral-rostral part of the cortex is highly hyperpolarized during this phase, stimuli entering the cortex during this phase are not likely to initiate a new wave.

V. Discussion

A. Information Coding by Cortical Waves

The initiation and propagation of cortical waves is a general property of sheets of neurons. It is possible, then, that the waves observed in turtle visual cortex with voltage sensitive dye and multielectrode methods are an artifact of the structure of the cortex. However, several studies from our laboratory have now suggested that information about visual stimuli is encoded in

the spatiotemporal dynamics of the cortical waves. Nenadic *et al.* [4] used a large-scale model of turtle visual cortex to show that information about the position and speed of visual stimuli is contained in the waves and can be decoded from the waves using a two-step Karhunen-Loeve procedure and Bayesian detection methods. The second paper in this series (Du *et al.* [5]) differed from the first paper in several important ways. First, the model used in the second paper and the current study explicitly incorporate the stochastic nature of neuronal firing. The model used by Nenadic *et al.* [6] was essentially deterministic and randomness was introduced by the unphysiological method of perturbing the spatial positions of individual neurons. Second, the model in [6] was relatively more inhibited and showed relatively poor wave propagation. By contrast, the model used in the current paper is less inhibited and wave propagation is obvious with different types of inputs. Third, the noise level used in the model in the current paper is relatively high and noise-evoked spiking occurred in the absence of input stimuli. This made discrimination tasks more difficult than they were in [4]. Fourth, the model in [6] had 801 geniculate neurons while the model in this and the preceding paper [5] had 201 geniculate neurons. Fifth, the method used for input discrimination in this paper combined a windowing technique and the Bayesian approach with a whitening filter, while the study in [4] did discriminations using the full 1 000 ms of the cortical response.

The fifth difference led to the important conclusion that the information content of the cortical responses varies as a function of time. Du *et al.* [5] found that the detectability of stationary stimuli decreased approximately linearly from chance levels at 0 ms to a peak detectability at about 200 ms. Detectability then gradually increased back towards chance levels by about 900 ms. This paper extends these results and shows that detectability of flashed stimuli and moving stimuli follows the same general time course.

B. Rate Versus Spike Time Codes

The relative efficiency of neural codes based on the average rate of neuronal firing and of codes based upon the precise occurrence of action potentials has been a matter of considerable debate over the past decade [8]–[11], and [12]. This study compared the effectiveness of rate and spike timing codes. Rate codes were produced by low-pass filtering the firing timing patterns of neurons in the large-scale model. Spike-timing codes were produced by forming a spike timing matrix for all of the neurons in the model. The results indicate that both rate and spike time codes provide for good discriminability of moving stimuli, but that spike timing codes were somewhat more effective. In addition to time code, spike timing has been reported to play an important role in spike timing dependent plasticity and learning [13], [14]. These results indicate the significance of spike timing in neural information processing.

C. Cellular Mechanisms Underlying Coding

Since the detectability of both stationary and moving stimuli varies as a function of time, it was interesting to correlate the concave shape of the probability of error curves with events occurring in the cortical model at different time periods. This analysis indicates that the cortical responses can be divided into three phases. The first phase consists of the initiation of the response and corresponds to the time period during which error probability is decreasing linearly. This phase occupies the time period during which the spatial pattern of geniculate afferents is established in the cortex. The second phase consists of wave propagation and corresponds to a period in which error probability is minimal, but then gradually increases. The third phase consists of the cessation of the wave and corresponds to the period in which error probability increases back to chance levels. Wang *et al.* [15] identified similar components of the responses to diffuse light flashes using the large-scale model of the cortex.

REFERENCES

[1] J. C. Prechtl, L. B. Cohen, P. P. Mitra, B. Pesaran, and D. Kleinfeld, "Visual stimuli induce waves of electrical activity in turtle visual cortex," *Proc. Nat. Acad. Sci. USA '94*, pp. 7621–7626, 1997.

[2] D. M. Senseman, "Correspondence between visually evoked voltage sensitive dye signals and activity recorded in cortical pyramidal cells with intracellular microelectrodes," *Vis. Neurosci.*, vol. 13, pp. 963–977, 1996.

[3] D. M. Senseman and K. A. Robbins, "Modal behavior of cortical neural networks during visual processing," *J. Neurosci.*, vol. 19, no. RC3, pp. 1–7, 1999.

[4] Z. Nenadic, B. K. Ghosh, and P. Ulinski, "Modeling and estimation problems in the turtle visual cortex," *IEEE Trans. Biomed. Eng.*, vol. 49, no. 8, pp. 753–762, Aug. 2002.

[5] X. Du, B. K. Ghosh, and P. Ulinski, "Encoding and decoding target locations with waves in the turtle visual cortex," *IEEE Trans. Biomed. Eng.*, vol. 52, no. 4, pp. 566–577, Apr. 2005.

[6] Z. Nenadic, B. K. Ghosh, and P. Ulinski, "Propagating waves in visual cortex: A large scale model of turtle visual cortex," *J. Computational Neurosci.*, vol. 14, pp. 161–184, 2003.

[7] H. L. Van Trees, *Detection, Estimation and Modulation Theory*. New York: Wiley, 1968.

[8] F. M. Rieke, R. deRuyter van Stevenick, D. Warland, and W. Bialek, *Spikes: Exploring the Neural Code*. Cambridge, MA: MIT Press, 1997.

[9] P. Dayan and L. F. Abott, *Theoretical Neuroscience: Computational and Mathematical Modeling of Neural Systems*. Cambridge, MA: MIT Press, 2001.

[10] R. C. deCharms and A. Zador, "Neural representation and the cortical code.," *Annu. Rev. Neurosci.*, vol. 23, pp. 613–647, 2000.

[11] W. Gerstner, A. K. Kreiter, H. Markram, and A. V. M. Herz, "Neural codes: Firing rates and beyound.," *Proc. Nat. Acad. Sci. USA*, vol. 94, pp. 12740–12741, 1997.

[12] A. Borst and F. E. Theunissen, "Information theory and neural coding.," *Nature Neuroscience*, vol. 2, pp. 947–957, 1999.

[13] T. Toyoizumi, J.-P. Pfister, K. Aihara, and W. Gerstner, "Generalized bienenstock-cooper-munro rule for spiking neurons that maximizes information transmission.," *Proc. Natl. Acad. Sci. USA*, pp. 5239–5244, 2005.

[14] Q. Liu, L. Pu, and M. Poo, "Repeated cocaine exposure facilitates LTP induction in midbrain dopamine neurons.," *Nature*, vol. 437, pp. 1027–1031, 2005.

[15] W. Wang, C. Campaigne, B. K. Ghosh, and P. S. Ulinski, "Two cortical circuits control propagating waves in visual cortex," *J. Comput. Neurosci.*, vol. 19, pp. 263–289, 2005.

Xiuxia Du received the D.Sc. degree in systems science and mathematics from the Department of Electrical and Systems Engineering, Washington University, St. Louis, MO, and the M.S. and B.S. degrees in electrical engineering from the Hefei University of Technology, Hefei, China.

She is currently doing research in proteomics at the Pacific Northwest National Laboratory, operated by Battelle for the Department of Energy. Her research interests include computational biology and linear and nonlinear dynamics of complex biological systems.

Bijoy K. Ghosh (S'78–M'79–SM'90–F'00) received the B.Tech. and M.Tech. degrees in electrical and electronics engineering from BITS, Pilani, India, in 1977 and IIT, Kanpur, India, in 1979, respectively. In 1983, he received the Ph.D. degree in engineering from the Decision and Control Group of the Division and Applied Sciences, Harvard University, Cambridge, MA.

Since 1983, he has been a faculty member in the Department of Electrical and Systems Engineering at Washington University, St. Louis, MO, where he is currently a Professor and directs the center for BioCybernetics and Intelligent Systems. His research interests are in multivariable control theory, machine vision, robotics, biological control systems, and systems biology. In 1993, he had been an UNDP consultant under the TOKTEN program and visited IIT. In 1997, he received the Japan Society for the Promotion of Science Invitation Fellowship for research in Japan and visited Tokyo Denki University and Mechanical Engineering Laboratory, Tsukuba City, Japan. He has also held short-term visiting positions at Osaka University, Osaka, Japan in 1992, the Tokyo Institute of Technology, Tokyo, Japan, in 1995, Padova University, Padova, Italy, in 2001 and Institut Mittag-Leffler, Djursholm, Sweden in 2003. He is a permanent Visiting Professor at the Tokyo Denki University, Tokyo, and in the spring of 2001 he visited the Electrical Engineering Department at Yale University, New Haven, CT.

Dr. Ghosh received the American Automatic Control Council's Donald P. Eckman award in recognition of his outstanding contributions in the field of Automatic Control in 1988. In 2000, he became a Fellow of the IEEE, for fundamental contributions in Systems Theory with applications to robust control, vision and multisensor fusion. He is presently an elected member of the Board of Governors of the IEEE Control Systems Society.

Philip S. Ulinski received the Ph.D. degree in zoology from Michigan State University, East Lansing, in 1968.

He is currently Professor and Chairman of the Committee on Computational Neuroscience at the University of Chicago, Chicago, IL. His research interests include the functional organization of the cerebral cortex and computational models of neural circuits.